Acta Biomaterialia xxx (xxxx) xxx

Contents lists available at ScienceDirect

Acta Biomaterialia

journal homepage: www.elsevier.com/locate/actbio

Magnesium incorporation into primary dental enamel and its effect on mechanical properties☆

Viktória K. Kis[a,b,*], Attila Sulyok[a], Máté Hegedűs[c], Ivett Kovács[d], Noémi Rózsa[e], Zsolt Kovács[c,*]

[a] Centre for Energy Research, H-1121 Budapest, Konkoly-Thege Miklós u. 29-33, Hungary
[b] Institute of Environmental Sciences, University of Pannonia, H-8200 Veszprém, Egyetem út. 10. Hungary
[c] Departement of Materials Physics, Eötvös Loránd University, H-1119 Budapest, Pázmány Péter sétány 1/a, Hungary
[d] Research Centre for Astronomy and Earth Sciences, Institute for Geological and Geochemical Research, H-1112 Budapest, Budaörsi út 45, Hungary
[e] Semmelweis University, Faculty of Dentistry, H-1088 Budapest, Szentkirályi u. 47, Hungary

ARTICLE INFO

Article history:
Received 29 April 2020
Revised 24 July 2020
Accepted 25 August 2020
Available online xxx

Keywords:
Primary dental enamel
Mg uptake
Nanoindentation
XPS
HRTEM
Nanostructure

ABSTRACT

Cross-sectional study of sound primary dental enamel revealed hardness zonation and, in parallel, significant change in the Mg content below the prismless layer. Mg content is known to play an important role in enamel apatite biomineralization, therefore, Mg ion exchange experiments were carried out on the outer surface of sound primary molars and on reference abiogenic Ca-phosphates using $MgCl_2$ solution. Effects of Mg incorporation on crystal/particle size, ionic ratio and morphology were compared and the observed changes were explained by parallel diffusion and dissolution/reprecipitation processes.

Based on depth profile analysis and high resolution electron microscopy of the Mg-exchanged dental enamel, a poorly ordered surface layer of approximately 10–15 nanometer thickness was identified. This thin layer is strongly enriched in Mg and has non-apatitic structure. Below the surface layer, the Mg content increased only moderately (up to ~3 at%) and the apatite crystal structure of enamel was preserved. As a common effect of the Mg exchanged volume, primary dental enamel exhibited about 20% increase of nanohardness, which is intrepreted by strengthening of both the thin surface layer and the region below due to the decreased crystallite size and the effect of incorporated Mg, respectively.

Statement of significance

Dental enamel is the most durable mineralized tissue in the human body, which, in spite to be exposed to extreme conditions like mastication and acidic dissolution, is able to fulfill its biological function during lifetime. In this study we show that minor component magnesium can affect hardness properties of human primary dental enamel. Then, through Mg incorporation experiments we provide an additional proof for the poorly ordered Mg-containing intergranular phase which has been recently observed. Also, we report that the hardness of dental enamel can be increased by ca. 20% by Mg incorporation. These results contribute to a deeper understanding of sound primary dental enamel structure and may inspire new pathways for assisted remineralization of enamel and regenerative dentistry.

1. Introduction

Magnesium is one of the most abundant cations in human body, it is involved in numerous biological processes like glycolysis, protein synthesis and activation of enzyme systems. The inorganic component of bone, biological apatite, which is nanocrystalline carbonated apatite [1], stores two third parts of the body's full Mg content, one third of which is exchangeable, providing stores for the maintainance of body's Mg homeostasis. Mg also plays an important role in the regulation of the crystallization of biological

☆ Part of the Special Issue on Biomineralization: From Cells to Biomaterials, associated with the BIOMIN XV: 15th International Symposium on Biomineralization, held at the Ludwig Maximilian University, Sept 9-13, 2019, organized by Wolfgang Schmahl and Erika Griesshaber.

* Corresponding author.
E-mail addresses: kis.viktoria@energia.mta.hu (V.K. Kis), kovacszs@metal.elte.hu (Z. Kovács).

https://doi.org/10.1016/j.actbio.2020.08.035

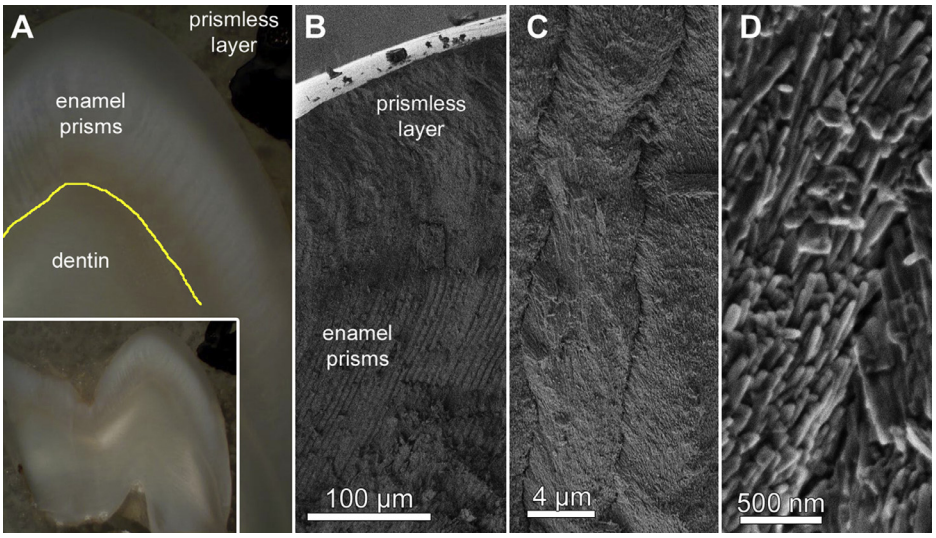

Fig. 1. Morphological overview of the cross section of the primary molar used in the nanoindenation tests. (A) Optical micrograph showing the dentine and the different zones of the enamel. SEM images showing (B) the enamel prisms and the prismless layer at the outer surface, (C) the prisms in the enamel and (D) apatite nanocrystals in the enamel prism.

calcium phosphates by exhibiting an inhibitory effect on crystal growth [2].

Dental enamel, is a special hard tissue made up by biological apatite, which also contains magnesium. Dental enamel is the most durable mineralized tissue in the human body, which is able to fulfill its biological function during lifetime. It is exposed to severe chemical and mechanical environmental effects without the ability of remodeling and with only very restricted capacity of remineralizing and repairing. Dental enamel is a biocomposite material, besides the main inorganic component hydroxyapatite (ca. 95 w%) it contains some water and enamel proteins as well [3]. The composition of the hydroxyapatite of enamel slightly differs from the stoichiometric $Ca_5(PO_4)_3OH$: it is carbonated, and besides magnesium, contains also other minor cations like sodium, potassium and strontium [4]. The basic inorganic building blocks of dental enamel are cca. 20–50 nm wide and up to micrometer long [3] hydroxyapatite nanocrystals which, similarly to bone, are organized in a hierarchical structure (Fig. 1) forming the enamel rods or prisms. The tiny amount of water and enamel protein is located between the nanocrystals and have crucial role in the stiffness of dental enamel. It allows a viscoelatic behaviour of dental enamel [5], which, together with the gradually changing misorientation of the adjacent nanocrystals [6] contributes to an effective blocking ability of crack propagation.

The nature and role of the approximately 0.2 w% magnesium in dental enamel has been unclear for a long time. It was thought to be hosted by an inorganic, probably apatitic phase [7,8], and also related to ameloblast activity and associated to the organic phase [9]. In agreement with this latter hypothesis, the distribution of magnesium in dental enamel was found to exhibit increasing concentration as function of distance from the outer surface and towards the enamel-dentin junction (EDJ) [10,11]. Recently several studies have focused on the spatial distribution and role of Mg in dental enamel. According to laboratory experiments, at higher synthesis temperatures Mg substitutes in crystallographic positions of apatite, either in Ca[1] [12,13] or in Ca[2] sites [14]. However, at physiological temperatures Mg has been found to accumulate in amorphous calcium phosphate (ACP), precursor phase during hydroxyapatite formation [2,15]. In rodent tooth enamel, atom probe tomography [16] supported the presence of an intergranular Mg-rich amorphous calcium phosphate rather than the Mg-Ca substitution in apatite. Similar poorly ordered, elongated Mg-rich precipitates were reported from mature human enamel as well, which were interpreted as a disordered precursor phase of enamel apatite [17]. In parallel to these studies on the nanoscale heterogeneities of dental enamel, rinsing experiments in hypersaline Mg solution, inspired by the geological process of dolomitization, revealed that mature human enamel is able to incorporate Mg inducing a simultaneous increase of microhardness and decrease of crystallite size in enamel apatite [18].

While the hierarchical microstructure of mature human enamel is well known e.g. [3], there are only a few recent works on the microstructure of sound primary enamel [19], most studies discuss pathological issues e.g. [20–22]. Sound primary enamel has a well preserved outer layer with a particular prismless microstructure, where enamel rods are absent (Fig. 1). While in mature enamel this prismless layer is either reduced to less than 5 µm or absent [23], in case of primary enamel its thickness in average is ca. 50–100 µm [23,24], but can reach values as high as 220 µm [24]. The distinct microscale organization of the nanocrystals in the outer layer of primary enamel implies different mechanical properties like fracture mechanism and hardness, and dissolution mechanisms and rates.

In this study we report on Mg incorporation into the outer surface of primary dental enamel by ion exchange experiments under controlled conditions, focusing on changes of the concentration, microstucture and strength characterized by nanohardness. As a reference, composition variation and nanohardness along a cross section of sound primary dental enamel were also determined. Furthermore, for better understanding the incorporation and effect of Mg on primary enamel properties, ion exchange experiments were performed on selected abiogenic nanomaterials. Then, based on analytical results we propose a mechanism of Mg incorporation and finally we report and interpret the effect of Mg uptake on hardness properties of primary enamel.

2. Materials and methods

2.1. Samples and treatment

Sound primary molars were selected for Mg ion exchange experiments. Chemical analysis by X-ray photoelectron spectroscopy (XPS) prior to the experiments indicated organic residues on the

Please cite this article as: V.K. Kis, A. Sulyok and M. Hegedűs et al., Magnesium incorporation into primary dental enamel and its effect on mechanical properties, Acta Biomaterialia, https://doi.org/10.1016/j.actbio.2020.08.035

Table 1
Summary of the abiogenic reference samples.

reference samples	origin	particle size and shape	crystallinity	composition	sample preparation
nAp	Synthetic, Berkeley Adv. Inc.	Nanoparticles, rod-like, size: 20–200 nm (100 nm[a])	nanocrystalline	$Ca_5(PO_4)_3(OH)$[a]	–
ACP	Synthetic, Sigma Aldrich	Nanoparticles, spherical, diameter: 10–100 nm (<150 nm[a])	Amorphous, minor contamination of monetite[b]	$Ca_2O_7P_2 \cdot H_2O$[a]	–
MAp	geological origin, Madagascar	Several cms	Well crystalline	$Ca_5(PO_4)_3(F, Cl,OH)$[c]	Crushed to powder of ca. <50 μm grain size

[a] nominal value given by manufacturer.
[b] according to our X-ray powder diffraction data.
[c] according to our TEM-EDS data.

surface of the molars (dominated by carbohydrate bonds) with only minor fraction of enamel mineral components (Ca, P) thus a pre-treatment cleaning procedure was applied. This procedure consisted of mechanical polishing of the molar surfaces with aqueous suspensions of Al_2O_3 of 1 μm, 300 nm and 50 nm grain sizes and subsequent ultrasonication in deionized water (DW). The procedure was repeated until a surface dominated by enamel mineral components was obtained which proved the successful removal of most of the organic residues. For Mg-ion exchange, the cleaned molars were then immersed into 5 ml of treatment solution in closed vessels at room temperature for 7 days. The studied primary molars originate from persons aged between 8 and 12 years and are voluntary donations. The research procedure is approved by the Ethics Committee of the Semmelweis University, Budapest (approval no. 84/2020).

For the reference cross sectional study, a molar sample was gently split into two parts and micromorphological observations were done on the freshly produced surface using scanning electron microscope. Then, one half of the molar was embedded in Dentacryl®, a two-component methyl methacrylate casting resin and left to solidify at room temperature for two days. Afterwards, the cross sectional surface was polished for nanoindentation measurements and chemical analysis.

Powder samples of Ca-phosphases of abiogenic origin were used as reference to assess the role of morphology and crystallinity of enamel apatite during Mg uptake. The abiogenic reference samples are summarized in Table 1. 500 mg of each powder was mixed with 5 ml of treatment solution and kept in closed vessel at room temperature for 7 days. To enable better contact between powder and solution, the vessel was hand-shaked twice daily. After treatment, sample was washed and settled three times and then dried at 36 °C.

Treatment solution was prepared at room temperature using anhydrous $MgCl_2$ (VWR) and DW, the final concentration of the solution was 50.69 g salt/100 ml, 5.3 M. The pH of the solution was set to 6.2, close to the physiological pH of sound saliva using TRIS (tris(hydroxymethyl)aminomethane, VWR). The advantage of using TRIS instead of the commonly used $Mg(OH)_2$ e.g. [18] is that (1) it does not affect the Mg^{2+} concentration of the solution and (2) apatite crystal structure, which is flexible both for cationic and anionic substitutions [25] do not incorporate TRIS molecules because of geometrical constraints.

2.2. Analytical methods

The morphology and crystallinity of the reference powder samples were checked using transmission electron microscopy (TEM) and the composition before and after treatment was followed using energy dispersed spectroscopy (EDS). EDS measurements were carried out using a Philips CM20 TEM with LaB_6 cathode working at 200 keV, and equipped with a Bruker EDS system (Quantax with XFlash Silicon Drift Detector). The chemical composition was analysed with 55 nm beam diameter and 100 s of counting time. Density and absorption correction were taken into account during quantitative TEM-EDS evaluation. High resolution TEM (HRTEM) was carried out using a JEOL 3010 TEM at 300 keV (LaB_6 cathode, 0.17 nm point-to-point resolution, UHR pole piece) equipped with GIF and an FEI Themis 200 G3 TEM with a C_s corrected objective lens (FEG, point resolution is around 0.09 nm in HREM mode) operated at 200 kV. Selected area electron diffraction (SAED) patterns were taken from areas of approximately 250 nm diameter. Suspension samples for TEM analysis were prepared using distilled water. A drop of the resulting suspension was deposited onto a standard ultrathin carbon coated copper TEM grid (Ted Pella). TEM samples from dental enamel were prepared using focused ion beam (FIB) milling with an FEI Scios 2 DualBeam System. Before FIB milling a thin amorphous carbon layer was deposited on the molar surface to prevent electrical charging of the surface. For rough milling 30 and later 16 keV Ga beam was used, and by reaching 100 nm lamella thickness the ion energy was reduced to 5 keV. Final polishing was done using 2 keV beam.

The surface composition of the primary dental enamel was measured using X-ray photoelectron spectroscopy (XPS). Primary molars were mounted onto sample holder/manipulator under ultrahigh vacuum conditions ($2 \cdot 10^{-9}$ mbar) and were exposed to 70 °C heat treatment for 48 h, which is the standard baking procedure of the applied vacuum system. Samples were adjusted by the two axis rotation ability of the manipulator such a way that the largest near flat area was illuminated and analyzed by X-rays. The size of measured areas varied between 3 and 5 mm in diameter, depending on the morphology of the molar samples. The photoelectron spectra were obtained using X-ray radiation (Al anode with water cooling, 15 keV excitation). Constant energy resolution of 1.5 eV was provided by a special cylindrical mirror analyser with a retarding field (type DESA 150, Staib Instruments Ltd.). All spectra were recorded with 0.1 eV energy steps. The XPS measurement yielded information on the average surface composition of the illuminated area. Detected lines (with its characteristic binding energy): F 1 s (686 eV); O 1 s (532 eV); Na Auger (497 eV); N 1 s (399 eV); Ca 2p (347 eV); Mg Auger (302 eV); C 1 s (285 eV); Cl 2p (199 eV); P 2 s (189 eV); Si 2 s (152 eV). The spectra were evaluated by applying the usual Shirley-background subtraction. Peak intensitites were derived by Gaussian-Lorentzian fitting for the peak shapes that provides the area of peaks. Elemental compositions were calculated from peak areas assuming homogeneous model. Sensitivity factors were calculated using reference spectra in [26]. Complex peak shapes were fitted applying more subpeaks where the subpeaks were associated to different chemical states (e.g. carbon subpeaks). The spectra were recorded in the 'as received' state of the molars, and after some ion sputtering of the enamel surface as well. The applied ion bombardment (1 keV Ar ion beam) was not expected to deteriorate the chemical

Please cite this article as: V.K. Kis, A. Sulyok and M. Hegedűs et al., Magnesium incorporation into primary dental enamel and its effect on mechanical properties, Acta Biomaterialia, https://doi.org/10.1016/j.actbio.2020.08.035

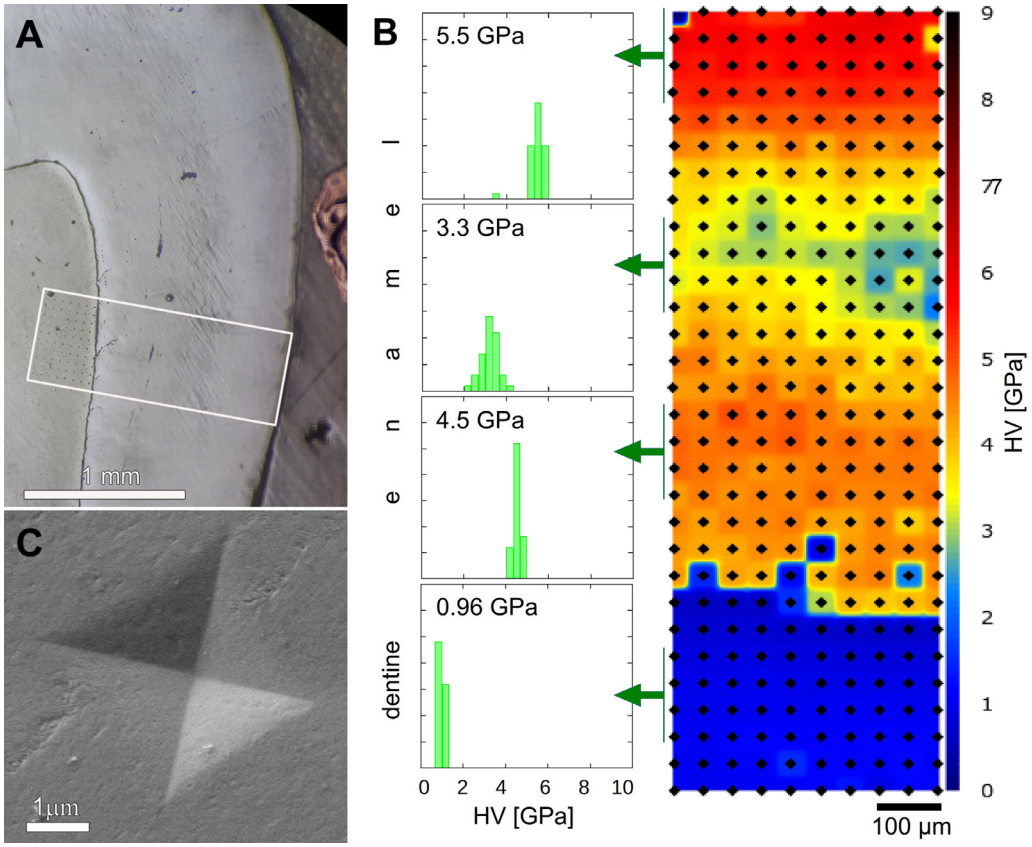

Fig. 2. (A) The area subjected to the nanoindentation tests is marked with white box on the optical micrograph. (B) Hardness map of the marked area with color coded Vickers hardness values. The insets show the hardness frequency distributions and the average hardness values of 4 × 10 tests at different selected depths in the enamel and in the dentin. (C) SEM image of a Vickers imprint in the enamel, showing its typical shape and size.

composition observed by XPS. The ion sputtering removed the majority of surface contamination on the enamel. On the other hand, the repeating cycle of ion sputtering-XPS made possible to reveal the in-depth distribution of observed components (XPS depth profiling).

Scanning electron microscopy (SEM) analysis was perfomed using an FEI Scios DualBeam System equipped with an Oxford SDD energy dispersive spectroscopy (EDS) detector. Before EDS analysis a thin Ti coating was sputtered onto the analysed surface which made possible long aquisition times needed for quantitative analysis without surface charging. During EDS line scan analysis an accelerating voltage of 8 keV was used.

Micro X-ray diffraction (XRD) measurements were performed using a Rigaku D/Max Rapid II diffractometer operating with CuK_α radiation generated at 50 kV and 0.6 mA. The diffractometer is equipped with MicroMax-003 third generation microfocus, sealed-tube X-ray generator and a curved imaging plate detector. To reduce the analysed area during diffraction measurement 100 μm sized collimator was used.

2.3. Nanoindentation

Nanoindentation tests were performed on the cross-section of a sound primary molar to map mechanical properties of the enamel and the dentin in a cca. 500 μm x 1500 μm section. The nanoindentation tests were placed in 10 × 30 positions (separated by 50 μm distance between the neighboring imprints) using an UMIS nanoindentation device with Vickers indenter by applying maximum load of 50 mN at a loading rate of 0.5 mN/s. The Vickers hardness (HV) from each nanoindentation was determined by the Oliver-Pharr method [27]. To characterize the change of the outer surface of the primary enamel after Mg treatment nanoindentation tests were performed in normal direction on the cleaned surface of primary molar before and after ion exchange experiments. These nanoindentation tests were placed in 10 × 10 positions covering a cca. 500 μm x 500 μm area on a selected nearly flat part of the curved surface of the molar.

2.4. Errors and statistical analysis

Elemental composition of primary dental enamel surfaces measured by XPS was averaged on 5–5 samples before and after $MgCl_2$ treatment. Elemental composition of powder samples measured by TEM-EDS was averaged on 10 independent aggregates of nanoparticles per sample in a similar way. Standard deviations of the measurements are indicated for both measurements. Nominally, elemental composition obtained from SEM-EDS had a ~0.1% relative error due to the adequately high acquisition time. Therefore, error bars were in range of symbol size and they were not indicated in the corresponding figure. However, the absolute values of the composition obtained by XPS and SEM-EDS may contain substantially higher errors.

3. Results

3.1. Mg distribution and nanohardness in sound primary enamel cross section

As the presence of a distinct prismless layer at the outer enamel surface is a specific microstructural feature of primary enamel [3,24], a primary molar with well preserved prismless layer was selected for cross sectional study (Fig. 1).

Please cite this article as: V.K. Kis, A. Sulyok and M. Hegedűs et al., Magnesium incorporation into primary dental enamel and its effect on mechanical properties, Acta Biomaterialia, https://doi.org/10.1016/j.actbio.2020.08.035

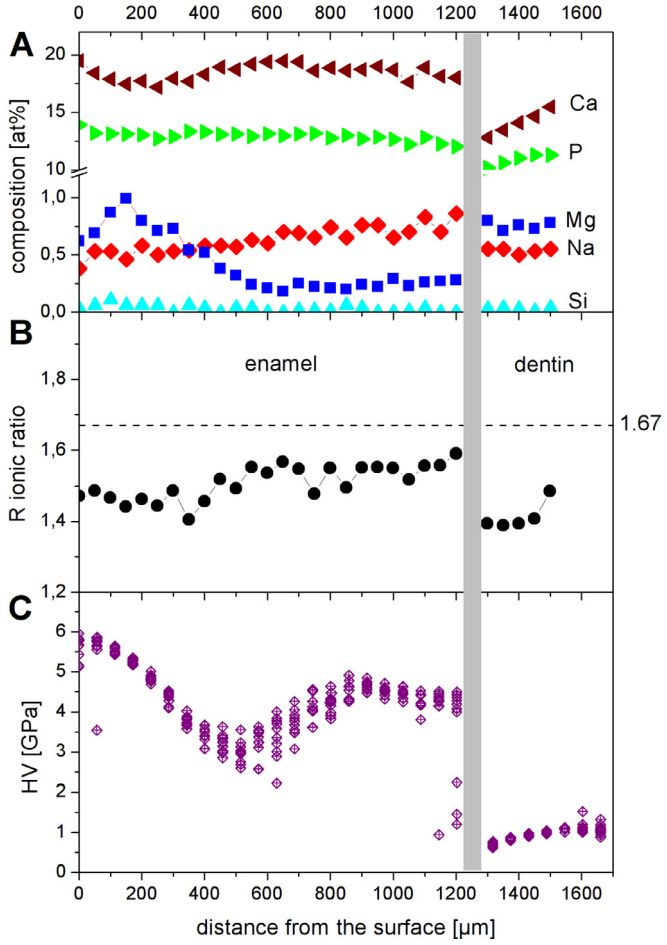

Fig. 3. (A) Compositional data obtained from SEM-EDS line profile analysis from the enamel surface towards the enamel-dentin junction and dentin. (B) R ionic ratio calculated from the SEM-EDS results and (C) hardness values obtained from nanoindentation tests near the same cross-sectional area shown on Fig. 2.

The results of the cross-sectional nanoindentation tests are shown in Fig. 2. Fig. 2a exhibits an optical image of the cross-sectional area in which the nanoindentation measurements were performed. The measured hardness values (see Fig. 2b) vary in the range of 6 and 2 GPa and a definite zonation can be observed for enamel. The highest values were measured in the outer 150 µm region with an average value over 5.5 GPa (see the local hardness frequency distributions for the various zones in the insets of Fig. 2b). Then the HV decreases gradually until reaching its minimum value (average 3.3 GPa) at around 600 µm from the enamel surface. After that, a moderate increase of HV can be observed up to cca. 4.5 GPa in a wider region at 800–1200 µm from the outer surface. Finally, at the EDJ the hardness drops drastically and it reaches about 0.95 GPa in the dentine. Fluctuation of the hardness measurements changed significantly between a reasonably small value of 5% to about 30% at specific distances from the surface (see also in Fig. 3). It is interesting to note that the variation of HV at a definite distance from the enamel surface is small, 5–10%, if the average HV is high. In the middle region (500–900 µm from the enamel surface), where well developed prisms were observed in the SEM micrographs (Fig. 1), the variation of HV was significantly larger, 25–30%. According to supplementary micro XRD measurements from the three regions of different nanohardness, only crystalline apatite was dectected (Figure S1).

Chemical composition by SEM-EDS line scan was determined just beside the nanoindentation imprints. Point analyses were located at cca. 50 µm from each other and the results of the line scan are plotted on Fig. 3. Main and minor components are plotted separately for clarity. The concentration of Ca and P, the main components of hydroxyapatite exhibit only minor relative changes. Ca content decreases from the outer surface in a cca. 150 µm zone, and for P, this tendency was observed through the whole thickness of the enamel down to the EDJ (Fig. 3a). Similar trend is known from the literature for mature enamel [11]. Regarding minor components, the concentration of Na increases monotonously from the outer surface (0.4 at%) towards the enamel dentin junction (0.8 at%), while the concentration of Mg has maximum value (1 at%) at ca. 150 µm from the outer surface. Then decreases gradually until reaching 800 µm distance from the outer surface (0.2 at%), and from here towards the dentin exhibits a very weak increase (up to 0.25 at%) (Fig. 3a). At the EDJ drastic compositional changes occur. Ca, P, and Na contents decrease by ca. 20%, 15% and 40%, respectively, while Mg content increases by ca 300%. These changes at the EDJ in tendency are similar to those reported for mature enamel [11] and indicate a different type of mineralized tissue, which exhibits similar properties to bone apatite rather to enamel apatite.

For crystalline calcium phosphates, the Ca/P ratio is a diagnostic parameter for composition based phase identification e.g. [12]. As biogenic apatites contain several subsitutional elements such as Na and Mg in the crystallographic position of Ca, and also Si in position of P, in the following we will use the ionic ratio $R = (c_{Ca}+c_{Mg}+c_{Na})/(c_P+c_{Si})$, where c denotes the atomic concentration of the corresponding elements. This ionic ratio R is plotted in Fig. 3b and a moderate increase can be observed from the enamel surface towards the EDJ, which is probably related to carbonate substitution in the PO_4 anionic site. In Fig. 3 it is also seen, that while P and Na concentration as well as the ionic ratio varies near linearly with distance from the outer enamel surface, the concentration curve of Mg exhibits markedly different shape. For comparison, hardness values corresponding to a given distance from the outer surface are plotted in Fig. 3c.

3.2. Mg ion-exchange experiments on dental enamel and reference materials

To investigate the ion uptake process and hardness variation of primary enamel in Mg rich environment, ion exchange experiments were carried out. First, the ability of primary dental enamel for Mg uptake was studied. Then, three reference materials (see Table 1) were subjected to the same experiment, according to the following considerations. nAp is synthetic nanocrystalline hydroxyapatite nanopowder, the shape and size of the crystallites match well with those of dental enamel apatite (as seen in the TEM images in Fig. 4). MAp is well crystalline apatite of geological origin, and as such, makes possible to evaluate the role of crystal size and highlight the effect of the nanocrystallinity during ion exchange. Finally, an amorphous nanopowder (sample name ACP) was also included in the experiments as well. As the atomic structure of ACPs are supposed to be built up by clusters of ca. 1 nm diameter with apatite-like local arrangement of Ca^{2+} and PO_4^{3-} ions [28,29], ACPs are suitable to check the effect of structural order on the Mg incorporation. The study of the amorphous nanopowder is also justified by recent studies, which point out the amorphous component of dental enamel [30,31] and relates Mg content to a highly disordered, amorphous phase [16,17]. These reference materials serve as pure standards during the study of Mg incorporation in biogenic apatite. TEM micrographs, HRTEM images and SAED patterns of the reference materials are seen in Fig. 4.

Please cite this article as: V.K. Kis, A. Sulyok and M. Hegedűs et al., Magnesium incorporation into primary dental enamel and its effect on mechanical properties, Acta Biomaterialia, https://doi.org/10.1016/j.actbio.2020.08.035

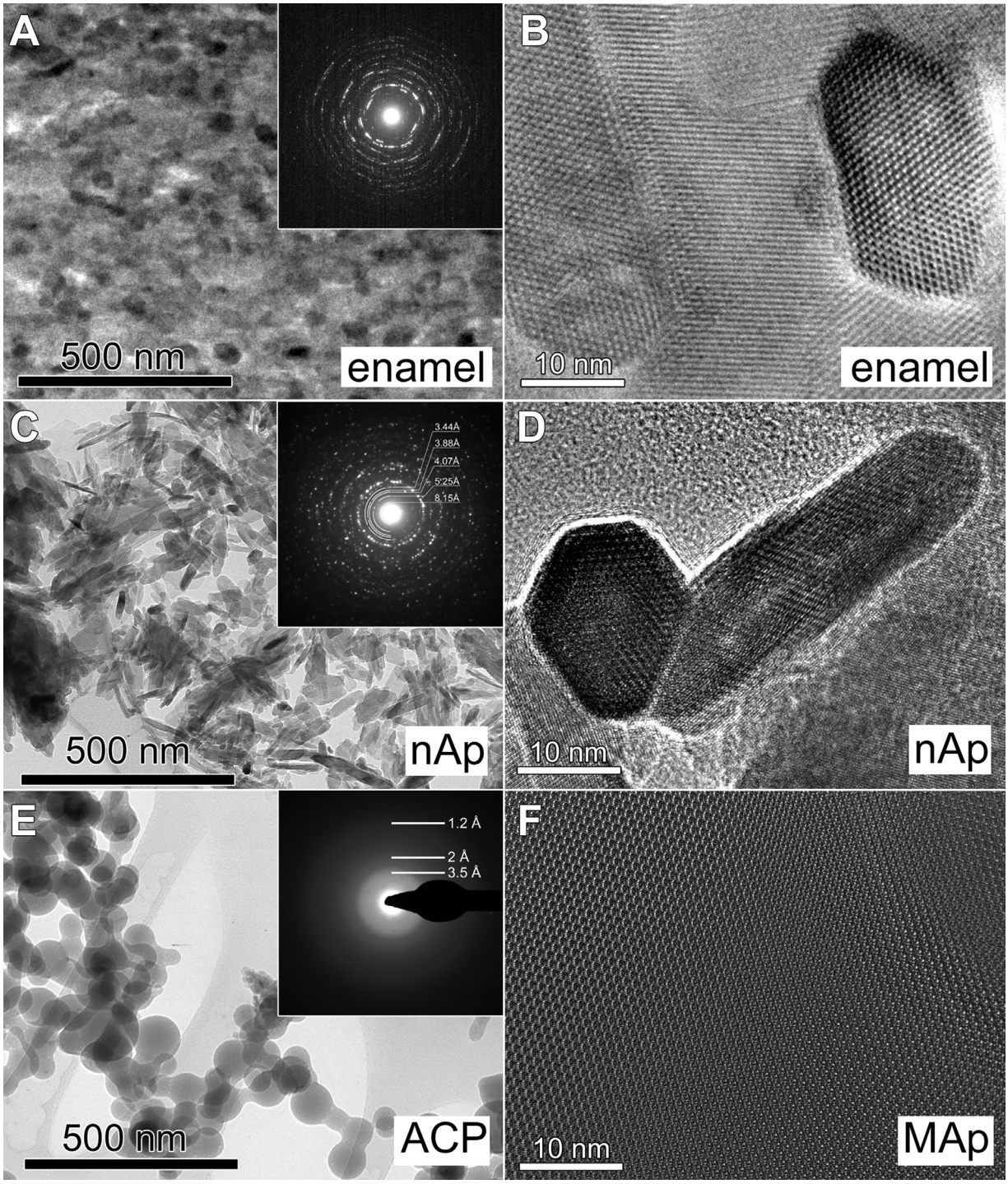

Fig. 4. TEM images of the studied enamel and reference Ca-phosphate nanomaterials. (A) primary dental enamel: bright field image with SAED pattern in the inset and (B) HRTEM image. (C) Nanocrystalline hydroxyapatite nanoparticles: bright field image with SAED pattern in the inset and (D) HRTEM image. (E) Amorphous calcum phosphate nanoparticles: bright field image and SAED in the inset. (F) HRTEM image of the MAp sample. The crystals in the HRTEM images of enamel, nAp and MAp samples are shown in the same crystallographic orientation. Note that the morphology and size of the hydroxyapatite nanocrystals in (D) are very close to that of the dental enamel apatites in (B).

3.2.1. Mg incorporation into primary dental enamel

The Mg incorporation into primary enamel was quantified by XPS. All dental enamel samples exhibited significant carbon content on the surface. Indeed, due to the high surface sensitivity of the XPS, all surface contaminations, due either to air exposure (mostly carbon compounds) or to insufficient mechanical cleaning procedure, were detected and additional efforts were needed for their separation. The carbon 1 s peak of XPS spectra is sensitive to the chemical bonding and the detected carbon signal can be decomposed to subpeaks (Figure S2). The surface contamination that usually consists of organic compounds with longer carbohydrogen chains and/or carbohydrates, can be distinguished from the C atoms with more oxygen bounds, like CO_3, based on their binding energies, which are 284.6 eV, 286.2 eV and 289.5 eV, respectively. Therefore, the identified organic carbon contamination was removed by initial Ar ions sputtering for 5–10 min until the

Please cite this article as: V.K. Kis, A. Sulyok and M. Hegedűs et al., Magnesium incorporation into primary dental enamel and its effect on mechanical properties, Acta Biomaterialia, https://doi.org/10.1016/j.actbio.2020.08.035

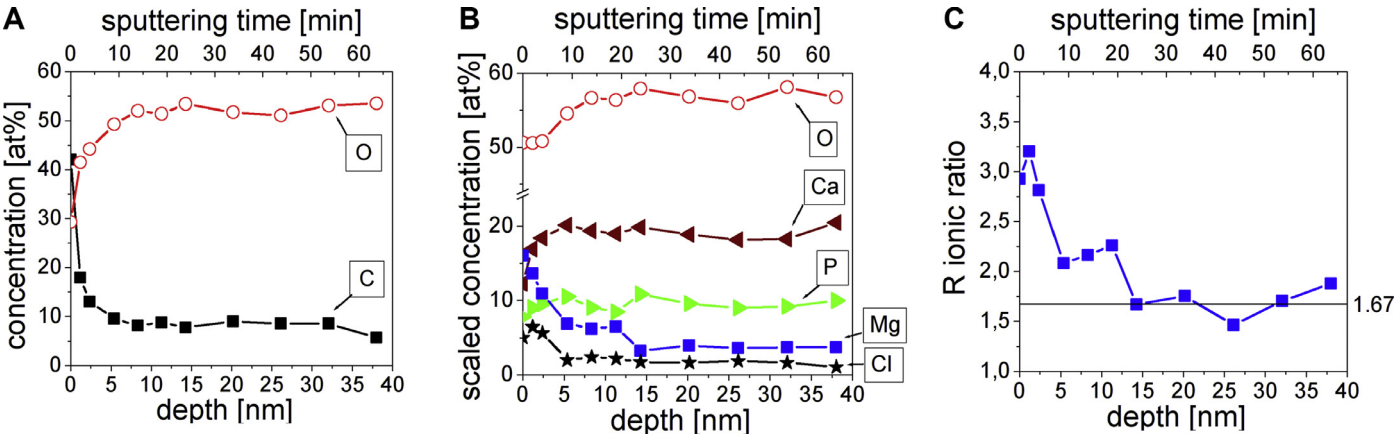

Fig. 5. (A) Depth distribution of C and O in primary molar enamel after $MgCl_2$ treatment determined by XPS profiling. (B) Depth distribution of enamel components (P, O, Ca, Mg and Cl) calculated from XPS analysis after removing C contamination. (C) Ionic ratio R as function of depth.

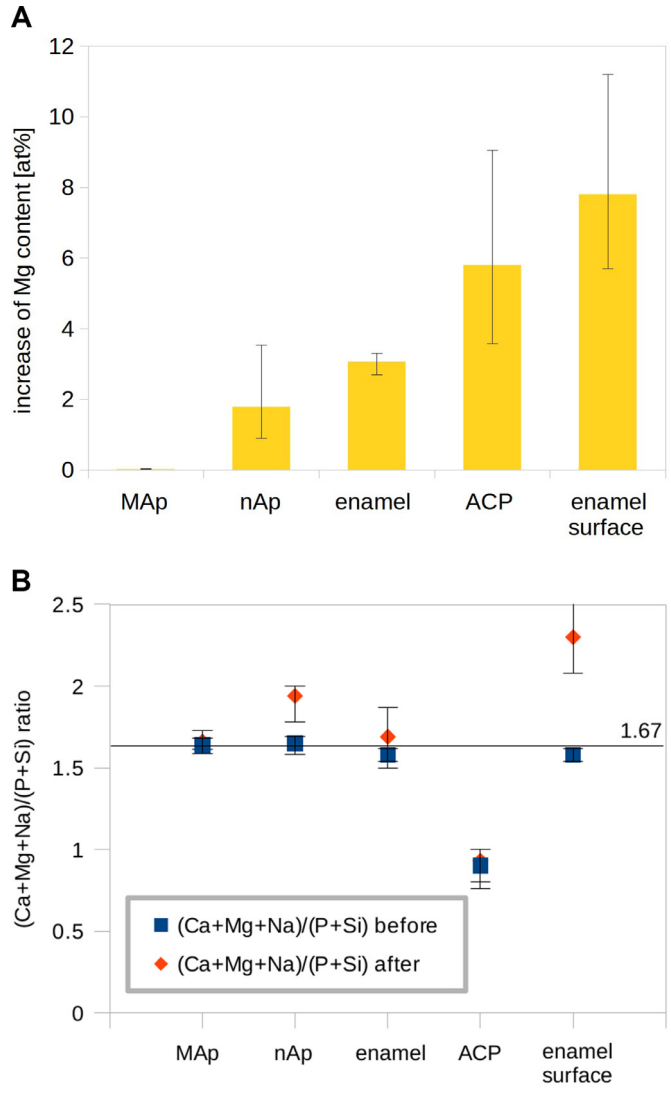

Fig. 6. Mg incorporation in primary molar enamel and the reference abiogenic Ca-phosphates. (A) Comparison of changes in Mg concentration measured in primary dental enamel and reference materials. (B) Comparison of changes in the R ionic ratio measured in primary dental enamel and reference materials. Values for abiogenic phosphates are averaged from 10 independent measurements. Error bars indicate the measured maximum and minimum values.

stable dental composition is reached, and the XPS measurements were performed afterwards. Regarding the remaining carbon signal, which was in the 10–20 at% range, the majority of the detected carbon was also simple surface contamination and carbon atoms with multiple oxygen bound was observed only in ~1%. (Figure S2). Composition of dental enamel was calculated from observed XPS signal after excluding the organic surface contamination. Table 2. shows the average composition of 5–5 samples before and after $MgCl_2$ treatment. Significant Mg incorporation into the surface of the treated dental enamel was demonstrated by the increase of the average Mg content from 0.3 to 8.1 at%.

Because of their identical binding energies, the CO_3 cannot be separated from carboxyl group ($O = C$–OH) in XPS analyses. Due to the organic environment of the enamel samples, some part of the carbon atoms with multiple oxygen bound, if not all, can be attributed to carboxyl group. Thus, the XPS analysis exhibits weak signal of possible CO_3, which implies only minor carbonate substitution in enamel hydroxyapatite in accordance with the literature [4].

To characterize the Mg incorporation into enamel apatite as a function of depth, XPS depth profiling was performed by successive Ar ion sputtering and XPS measurements. The XPS depth profile of a selected primary molar dental enamel sample after $MgCl_2$ treatment can be seen in Fig. 5. The sputtering time between two XPS measurements was 2 min at the first few sputtering steps, later it increased to 5 min and then to 10 min. The overall sputtering time of 64 min was estimated to remove approx. 40 nm from the enamel surface (based on other experiments with known thickness removal), however the sputtering was not even because of the surface curvature. As seen in Fig. 5a, the applied ion sputtering of the top 3 nm layer significantly reduced the carbon content from 40–60% to 5–10%, but all the contamination cannot be removed perfectly because the surface curvature and shape of the molars prevent an even sputtering of the analysed surfaces (the surface topography of a real dental shape reaches macroscopic scale with micrometer sized features while the material removal by sputtering measurement occurs on the nanometre scale). The decrease of carbon concentration with depth is in agreement with the fact that the information depth of photoelectrons is ~3 nm. Transient behavior of the remaining surface contamination was visible in the profiles of all the measured components, therefore we plotted in Fig. 5b these components by removing the carbon content and renormalizing them to 100% (Table S1).

The O distribution after the removal of C contamination (see Fig. 5b) gives a reasonable value in the 52–57 at% range, which approximates well the stoichiometric amount in apatites (57–62 at%).

Please cite this article as: V.K. Kis, A. Sulyok and M. Hegedűs et al., Magnesium incorporation into primary dental enamel and its effect on mechanical properties, Acta Biomaterialia, https://doi.org/10.1016/j.actbio.2020.08.035

Table 2
Elemental composition (at%) of primary dental enamel and the R ionic ratio showing the Mg ion incorporation due to $MgCl_2$ treatment, as measured by XPS averaged on 5–5 samples, standard deviation is given in round brackets.

	F	Na	P	N	O	Ca	C	Si	Mg	Cl	Ionic ratio
untreated	1.3 (0.1)	1.0 (0.1)	10.1 (0.2)	6.1 (0.3)	59.6 (1.0)	17.0 (0.4)	2.0 (0.2)	1.5 (0.2)	0.3 (0.2)	0.9 (0.1)	1.58 (0.11)
$MgCl_2$ treated	2.9 (0.1)	0.5 (0.1)	10.9 (0.2)	0.5 (0.1)	51.6 (1.0)	20.6 (0.4)	0.4 (0.2)	1.8 (0.2)	8.1 (0.2)	2.7 (0.1)	2.3 (0.13)

The diagram clearly shows the penetration of Mg and Cl into the enamel due to $MgCl_2$ treatment. Both elements seem to be present at higher concentrations near to the surface and stabilize at depths beyond 10–15 nm. Other components (Ca and P) show also reasonable values. Based on the variation of the Mg concentration in Fig. 5b, a Mg rich layer formed close to the surface (0–15 nm) with about 7–8% Mg average content and a thicker layer with about 3–4% Mg content was revealed at higher depths (>15 nm). Mg and Cl correlate quite well (correlation coefficient 0.81 for the whole depth range, Figure S3), their ratio varies between 1.8–3.5 giving an average Cl:Mg = 0.4, which falls far from the stoichiometry of $MgCl_2$. This fact supports that Mg (and also Cl) incorporated into the surface of enamel apatite and no precipitation of chloride has occurred. Similarly, compositional comparison with the apatite structure after the Mg-exchange can also be made using the R ionic ratio. Fig. 5c indicates that at smaller depths and especially within the upper few nanometers from the enamel surface the ionic ratio is significantly higher (between 2 and 3.2) than the stoichiometric ionic ratio for apatite structure (1.67), implying a different atomic environment. At depths >15 nm, the ionic ratio converges to the nominal value of the apatite structure, which supports that the enamel apatite crystal structure is preserved and Mg is incorporated into the structure as substitutional atom.

3.2.2. Mg incorporation into abiogenic Ca-phosphate reference samples

The Mg incorporation into the abiogenic phosphate reference samples was followed by TEM-EDS, the results, together with the XPS results of Mg-exchanged primary molars, are presented in Fig. 6. Two parameters were investigated, namely the increase of Mg-content and the change of the R ionic ratio. In case of dental enamel, the results at shallow depth (labeled “enamel surface”) and depth lower than 15 nm (labeled “enamel”) were plotted separately. For abiogenic phosphates, the total increase of Mg concentration was the highest in case of amorphous (ACP) sample, while the Mg uptake of the nanopowder (nAp) was between 1 and 4 at% and that of the well crystalline MAp sample was negligible during the duration of the experiment.

The morphology, particle size and crystallinity of the nanopowders and the dental enamel after the ion-exchange experiment was studied using TEM (Fig. 7). Bright field image of the Mg-treated dental enamel surface do not exhibit noticeable changes (Fig. 7a). However, careful observation at higher magnification (Fig. 7b) reveals a cca. 5–15 nm thick layer (depending on the position) on the surface, which, according to the Fourier transforms, has a poorly ordered/amorphous structure. The measured thickness of the poorly ordered surface layer on the HRTEM images coincides well with the thickness calculated for the Mg-rich surface layer based on depth profile analysis. Below this surface layer, apatite nanocrystals of the enamel are clearly recognizable on the HRTEM images. The transition between the surface layer and the enamel apatite crystals is continuous. Bright field and HRTEM images of the treated nAp nanocrystalline sample (Fig. 7c,d) show some needle-like apatite nanocrystals. The length of these nanocrystals is substantially longer than in the untreated case (compare with Fig. 4c), It can reach up to 150 nm and their width does not exceed 10 nm, so most of them contain only 5–8 atomic planes in width. These morphological features imply that these needle-like nanocrystals were grown during the Mg treatment.

The measured interplanar spacings on HRTEM images of both dental enamel and nAp are consistent with apatite, supporting that no new crystalline phase appeared during Mg-treatment in these samples. The ACP sample, according to SAED (Figure S4), remained amorphous with typical particle size below 100 nm. In the bright field image, a new type of irregular shaped nanoparticles were observed (indicated by white arrows in Fig. 7e), which decomposed very rapidly under the electron beam, producing bubble-like features. At the same time, more stable nanoparticles similar to the original ACP sample were also observed (black arrows in Fig. 7e). In summary, according to TEM observations, none of the three samples, either nanocrystalline or nanoparticles, contain a new crystalline phase after Mg treatment, however, Mg incorporation was accompanied by slight morphological changes on the nanoscale.

3.3. Nanoindentation on primary dental enamel surface before and after Mg uptake

To investigate the effect of Mg incorporation on the nanohardness properties, a primary molar sample was cut in two parts and one half was subjected to the experiment and the other half was kept as a reference. In this way the effect of individual variations of either the composition or the thickness of the prismless layer could be excluded. Nanoindentation tests were made on the Mg-exchanged enamel surface, consisting of a 10 × 10 array of individual HV measurements and the frequency distribution of the tests was compared to that of the untreated enamel surface (Fig. 8). Hardness distribution of the untreated surface shows a maximum at about 5.0–5.5 GPa, which is comparable to the typical hardness (5.5 GPa) measured in the cross section in the outer 150 µm thick layer of the untreated enamel (c.f. Fig. 2b).

However, in certain areas (see the corresponding hardness map in Fig. 8) significantly lower values were also measured. We suppose that the uneven surface morphology and possible residual surface contamination might deteriorate the hardness results in these locations. Therefore the maxima of the hardness distributions of the treated and untreated samples were compared to characterize the effect of $MgCl_2$ treatment on the mechanical behavior of dental enamel. As seen in Fig. 8, maximum of the frequency distribution exhibits an approximately 20% increase in the nanohardness after Mg-treatment with respect to the untreated surface, indicating that the treated surface layer become harder due to the Mg ion incorporation.

4. Discussion

Cross sectional study of a pristine sound primary dental enamel indicates hardness zonation from the enamel outer surface towards the EDJ (Fig. 2 and 3). At the outer 150 µm zone (prismless layer) of the enamel the hardness was the highest reaching 5–6 GPa, then it decreased gradually to a minimum of about 3.3 GPa at about 600 µm depth. Finally, the hardness moderately increased up to 4 GPa towards the EDJ. In parallel to the strong hardness variation in the interior of the cross section (with prisms), Mg content decreased gradually from 1% to 0.2 at% and then slightly increased to 0.25 at% towards the EDJ (Fig. 3c). Cuy et al. [11] performed cross

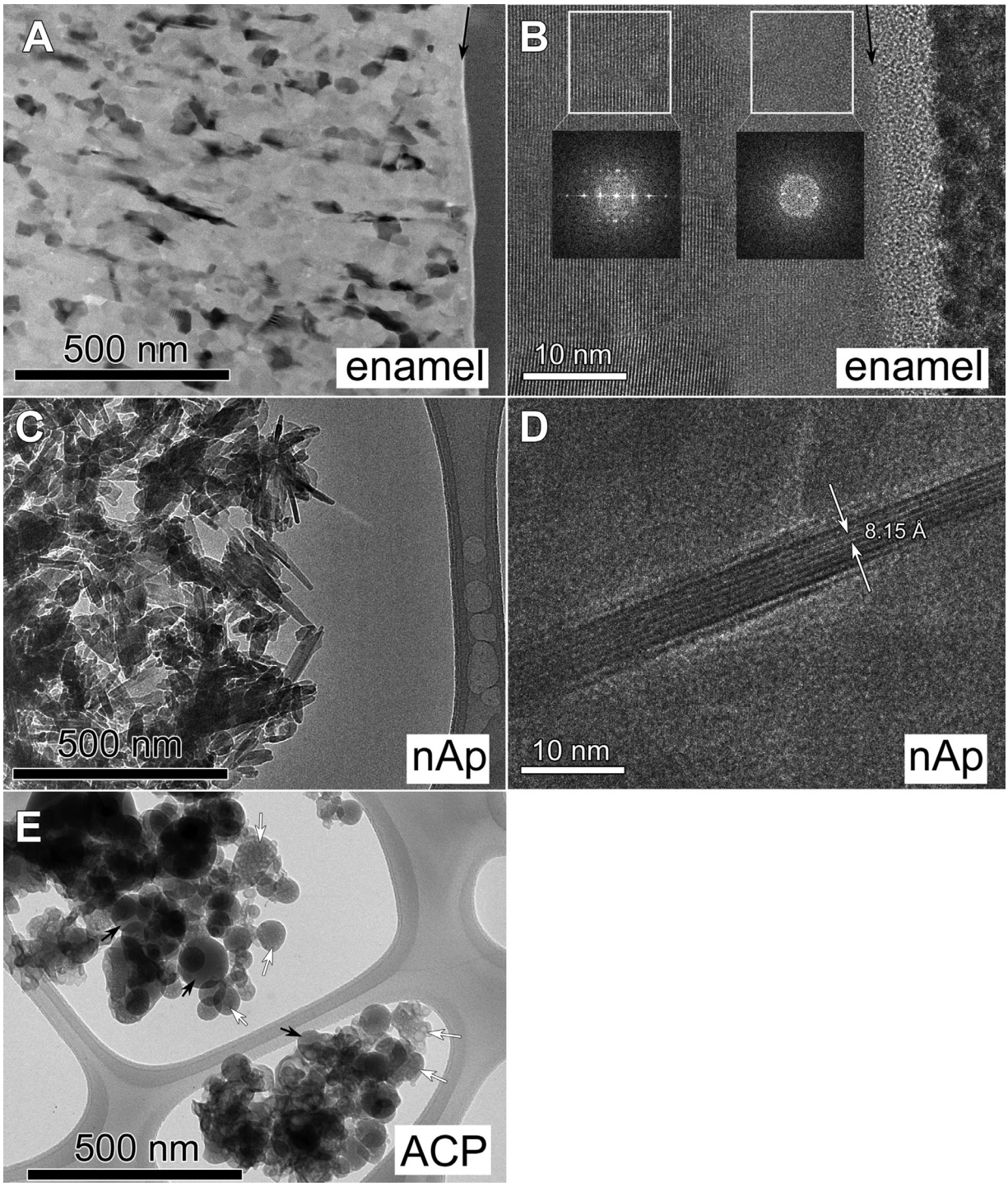

Fig. 7. TEM images of the studied samples after Mg exchange. (A) Bright field image and (B) high resolution image of Mg treated primary dental enamel. Black arrows indicate the outer surface of the enamel. FFTs are made from the indicated areas. (C) Bright field image and (D) HRTEM image of nAp nanocrystalline hydroxyapatite nanoparticles. (E) ACP nanoparticles. White arrows indicate newly formed nanoparticles with bubble-like features due to electron irradiation, black arrows indicate residual particles (see Fig. 4e), which are less sensitive to electron beam.

sectional measurements on three sections of three mature molars of different anatomic positions. According to their results, there is a general tendency of decreasing hardness from the enamel surface towards the EDJ, however the shape of the hardness and modulus profiles exhibits high variety even in case if section and anatomic position coincide. Our measurements have been performed on primary enamel, with well developed prismless layer, and the highest hardness was detected where the prismless microstructure occurred. In addition, high Mg concentration was measured in this outermost part of the enamel, which is unreported before. Thus, we cannot directly compare our hardness results to [11], however, based on microstructural considerations, the ca. 250–1200 μm interval in our measurements may correspond to their measurement interval and similar tendencies can be recognized. These results point out that besides changes in the average chemistry (especially in the Mg concentration), changes in microstructure and prism

Please cite this article as: V.K. Kis, A. Sulyok and M. Hegedűs et al., Magnesium incorporation into primary dental enamel and its effect on mechanical properties, Acta Biomaterialia, https://doi.org/10.1016/j.actbio.2020.08.035

alignment may affect hardness properties of dental enamel [6,11]. Therefore, we focus on the unique outer prismless layer of primary dental enamel in the following and we use the outer surface of the cross-sectional measurements as a kind of reference for the Mg exchange measurements.

Previous investigations on Mg exchange indicate that Mg is able to incorporate into synthetic nanocrystalline hydroxyapatites during coprecipitation [13,14,32] and ion-exchange reactions [33–35]. In a recent paper it has been proven that mature human dental enamel is also able to uptake Mg, which process is accompanied by the measurable changes of physical properties, e.g. microhardness of enamel [18]. Therefore, Mg uptake and incorporation, and the effect of Mg on structural changes in sound primary molars and pure abiogenic reference Ca-phosphates are discussed as follows.

4.1. Mg incorporation

According to the present ion exchange experiments, the Mg uptake ability of primary dental enamel falls between that of nanocrystalline hydroxyapatite and ACP (Fig. 6a). There is a general agreement in literature that at low temperatures (physiological/room temperature), nanocrystalline hydroxyapatite has only a restricted ability to incorporate Mg, with an upper limit of 3–7 mol% depending on experimental conditions (ion-exchange or precipitation, solution concentration, pH) [2,13,35]. ACP, on the contrary, is able to incorporate larger amount of Mg, up to 20–30 at% [2,36]. This behavior of Mg can be explained by the geometrical misfit of Mg^{2+} in the apatite Ca-positions caused by the relative size difference of the cations and implies the well known role of Mg as crystal growth rate regulator in both synthetic and biogenic apatites [15,2]. Our TEM-EDS data on Mg incorporation into nanocrystalline hydroxyapatite and ACP match these observations well. The total increase of Mg concentration was found to be the highest in case of amorphous (ACP) sample, while the nanocrystalline powder (nAp) exhibited moderated Mg uptake and, in parallel, the compositional change of the well crystalline sample was negligible during the duration of the experiment.

Basically two parallel processes take place during the $MgCl_2$ treatment of different samples. Mg ions incorporate into the existing crystalline/amorphous structure either by diffusion or by dissolution and reprecipitation. The first process preserves the atomic structure and can only change R slightly, however, the second process can lead to different R values and to an altered/new non-apatitic atomic structure. Thus, the R ionic ratio provides a suitable tool to distinguish between Mg uptake by crystal structural substitution via diffusion and by dissolution and reprecipitation. In our experiments the R ionic ratios in the MAp and ACP samples coincide well with the nominal values (1.67 and 1, respectively) and remain unchanged during Mg treatment. In case of the highly stable well crystalline, stoichiometric (defect free) F-apatite (MAp) unchanged R and nearly zero Mg uptake imply unchanged structure and crystal chemistry. In ACP, the mobility of the atoms is significantly higher than in crystalline samples, and thus considerable amount of Mg incorporates rapidly by diffusion, reducing the rate of the dissolution process by reducing the Mg concentration difference at the ACP-solution interface. The atomic structure of the resulting Mg-rich ACP does not change with respect to the untreated ACP. In case of the nanocrystalline powder sample (nAp), diffusion into the stable stochiometric (defect free) structure is much less efficient than for ACP. Therefore, the dissolution and reprecipitation become dominant processes leading to the formation of a new surface layer enriched in Mg, similar to the few nm thick interphase which forms on the surface of apatite nanocrystals in pure aqueous medium [37]. As no new crystalline phase was observed in nAp during TEM study (Figs. 7c and 7d), it can be concluded that the increased ionic ratio from $R = 1.67$ to 1.94 is due to the high volume fraction of this Mg-rich surface layer, which, according to R, has non-apatitic structure. At the same time, however, the formation of a minor amorphous phase cannot be excluded in this nanocrystalline sample.

The increase of Mg content in the primary dental enamel was investigated up to several tens of nanometer depth from the $MgCl_2$ solution treated surface. Based on the change of the R ionic ratio in the enamel, a dissolved and reprecipitated near surface layer of cca. 10–15 nm thickness with an altered atomic structure and 8 at% average incorporated Mg content was observed, while at larger depths the apatite crystal structure prevailed with an enriched Mg content. The increase of Mg content in primary dental enamel at larger depths was somewhat larger (about 3 at% in average), than in case of the reference hydoxyapatite nanopowder (1.78 at% in average), however, the increase of ionic ratio of nAp surpassed that of the primary dental enamel (Fig. 6b). The different behavior of nAp and dental enamel can be explained by separating the surface effect in case of enamel measurements. The 10–15 nm thick surface layer of the enamel exhibited comparable amount of Mg uptake to ACP indicating that the structure of both the newly formed enamel surface and ACP allows high atomic mobility. Though, difference in the ionic ratios ($R>2$ and $R = 1$ for enamel surface and ACP, respectively) indicate that the newly formed enamel surface layer has dissimilar atomic structure to the ACP. Dissolution and reprecipitation in this enamel surface layer lead also to the formation of smaller and less ordered Mg-containing phase, which is reflected by the morphological changes recorded by HRTEM (Fig. 7b). Similar morphological changes were observed in hydroxyapatite nanopowder with increasing Mg content by Ren et al. [13].

It is surprising that primary dental enamel in larger depths incorporated more Mg than the nAp sample (Fig. 6a). The HRTEM images indicate that the crystal size and morphology is practically the same for the pristine dental enamel and hydroxyapatite nanopowder (Fig. 4). In case of the nanopowder a large specific surface of the nanoparticles allows efficient ion-exchange between solution and particles, implying higher Mg uptake than in case of the surface of a molar, which can be considered as a compact ceramics. One possible explanation for the measured high Mg-incorporation data down to at least 40 nm depth can be the presence of the poorly ordered Mg-containing phosphate phase in between the enamel apatite nanocrystals, as deduced from atom probe tomography [16,17]. We presume that this phase behaves like a channel for migrating Mg ions allowing their penetration towards the inner pristine parts. Similar to the ACP, this poorly ordered phase may preserve its structure and R ionic ratio, while it is able to incorporate large amounts of Mg. The size of these Mg-rich precipitates in dental enamel ranges from ten up to several tens of nanometres [16,17], and they present a notable volume fraction in the dental enamel, which is in agreement with the measured effect. Additionally, the initial $R<1.67$ non-stoichiometry of the enamel indicates the presence of defects (e.g. Ca-vacancies [38]) in apatite structure, i.e. atomic environments with easy accumulation points for Mg ions. Diffusion of Mg into these vacancy positions can also increase the overall R value of the treated enamel. According to Figs. 6b and 5c, the R ionic ratio increased slightly (however within the standard deviations of the XPS measurements) in case of primary dental enamel, but in less extent than in case of nanocrystalline hydroxyapatite, and have not exceeded the stoichiometric value 1.67 for apatite structure. This observation is in agreement with a diffusion caused Mg enrichment in both enamel apatite crystal structure and poorly ordered phosphate phase of the enamel, the latter has also been proposed for pristine enamel in previous works [16,17].

Please cite this article as: V.K. Kis, A. Sulyok and M. Hegedűs et al., Magnesium incorporation into primary dental enamel and its effect on mechanical properties, Acta Biomaterialia, https://doi.org/10.1016/j.actbio.2020.08.035

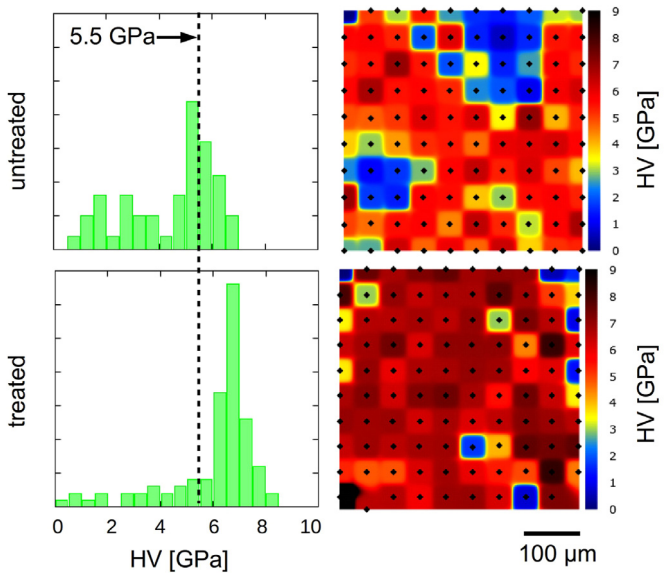

Fig. 8. Hardness frequency distributions and hardness maps obtained on the outer surface of treated and untreated molar enamels, respectively. The maximum hardness measured at the cross-section of the untreated molar enamel (presented in Fig. 2) is indicated by dotted line. The maximum hardness value has shifted due to the $MgCl_2$ treatment.

4.2. Implications for mechanical properties

Mg functions in enamel as an impurity during apatite biomineralization. Impurities may operate, in general, either as promoters or inhibitors during crystal growth. Inhibitor impurities are segregated by the atomic processes of the crystal growth and accumulate on growing crystal facets and grain boundaries [39]. Thus, Mg and other impurities have an important role during the crystallization of enamel apatite and concentrate naturally along grain boundaries between the apatite nanocrystals [16,17]. Such an intergranular layer with equilibrium thickness on the order of nanometer can strongly influence mechanical properties in such a ceramic like, bulk structure [40] that dental enamel has [41]. Our study indicate that the Mg content in enamel can be further increased by laboratory methods close to the treated surface. In details, the present Mg exchange experiments in primary dental enamel induced large concentration (~8 at%) and also structural changes in a ~10–15 nm thin surface layer and moderate concentration changes (~3 at%) without structural alteration below this layer at least three times larger depths. In previous work [18] microhardness measurements were performed on Mg exchanged surface of mature human molars. The authors attributed the measured minor hardness increase to a decrease of crystallite size and the related Hall-Petch effect. According to our HRTEM study, nanocrystal refining and amorphisation took place only in the thin surface layer and the size of nanocrystals remained unchanged beneath this layer. As in our experiments the nanoindentation tests in the enamel reached approx. 600 nm indentation depth (~1/7th of the diameter of the imprint, see Fig. 2c) at the applied 50mN maximum load, the thin surface layer might have only minor effect on the measured HV. Instead, the observed hardness increase after the Mg treatment can be at least partially attributed to the Mg incorporation into the deeper region below the surface layer. In this region of the enamel, Mg incorporation into both the apatite nanocrystals and the intergranular amorphous layer [16,17] can increase the hardness due to the following effects.

On one hand, the 10% higher melting point of the equilibrium MgO phase with respect to the melting point of the isostructural CaO phase implies an increased binding energy and thus a higher strength of Mg-O bonds with respect to Ca-O bonds. Considering the binding energy, direct calculations provide an estimate of Young's modulus for amorphous materials as function of composition [42]. As yield strength and HV are directly related to the elastic moduli [43], Ca to Mg substitution in an unchanged atomic structure (i.e. fraction of Ca-O bonds are replaced by Mg-O bonds) predicts an increased hardness. However, based on our average Mg incorporation data, this effect explains only a small hardness increase (<1%) in the intergranular amorphous layer of dental enamel. On the other hand, if the nonstoichiometric apatite nanocrystals of the untreated enamel approach stoichiometry after the Mg treatment, vacancy like point defects in Ca sites of the enamel apatite structure [38] diminish with Mg incorporation. Based on first-principles plane-wave calculations, the elastic moduli of the Ca-vacancy containing apatite are about 10–60% lower than those of the vacancy free apatite crystals, depending on the crystallographic position of the vacancy [44]. This anticipates that lower number of vacancies, i.e. composition approaching to stoichiometry, can increase hardness in enamel apatite. Therefore, our results (cf. Fig. 3a and 3b) indicate that the increased hardness in the outer prismless layer of the primary enamel cross section should have a structural origin, which explanation remains an open question. Whereas, the vacancy filling mechanism of Mg can explain the magnitude of the observed hardness increase at the outer surface of the primary enamel.

5. Conclusions

Mg incorporation into the prismless layer of sound primary enamel was studied by various methods, such as XPS, TEM and nanohardness tests. For comparison, Mg incorporation in pure abiogenic Ca-phosphates was investigated by carrying out the same ion exchange experiment and the effect of crystal size, morphology and crystallinity was studied. As a reference, composition variation and nanohardness along a cross section of sound primary dental enamel were also determined and these results indicate that both Mg content and microstructure affect enamel hardness in the outer prismless layer.

After Mg treatment of dental enamel, depth profile analysis and HRTEM allowed to distinguish two zones near the enamel surface. A surface layer of approximately 10–15 nanometer thickness proved to be strongly enriched in Mg with non-apatitic atomic environment. Below this surface layer the apatite crystal structure of enamel preserved with a moderately increased (in average 3 at%) Mg content. By comparing these changes with compositional changes of the abiogenic reference samples, two parallel processes, namely (1) incorporation via dissolution and reprecipitation and (2) direct incorporation by diffusion, were concluded in nanostructured apatites.

The increased Mg concentration in the dental enamel surface was followed by a notable increase of nanohardness (cca. 20%). Hardness increase was explained in part by the decreased crystallite size in the thin surface layer due to the inhibitory effect of Mg on reprecipitation and additionally by the effect of Mg, which diffused into larger depths and incorporated both into the apatite nanocrystals and the intergranular layers in between them.

Declaration of Competing Interest

The authors declare that they have no known competing financial interests or personal relationships that could have appeared to influence the work reported in this paper.

Acknowledgements

This work was supported by the National Research, Development and Innovation Fund Office, Hungary, grant number K-

125100. VKK is indebted to the János Bolyai Fellowship of the Hungarian Academy of Sciences and the ÚNKP-19–4 New National Excellence Program of the Ministry for Innovation and Technology. The work of ZsK was completed in the ELTE Institutional Excellence Program (1783–3/2018/FEKUTSRAT) supported by the Hungarian Ministry of Human Capacities. Electron microscopy facility at Centre for Energy Research was granted by the European Structural and Investment Funds, grant no. VEKOP-2.3.3–15–2016–00002.

Supplementary materials

Supplementary material associated with this article can be found, in the online version, at doi:10.1016/j.actbio.2020.08.035.

References

[1] J.D. Pasteris, B. Wopenka, J.J. Freeman, K. Rogers, E. Valsami-Jones, J.A.M. van der Houwen, M.J. Silva, Lack of OH in nanocrystalline apatite as a function of degree of atomic order: implications for bone and biomaterials, Biomaterials 25 (2004) 229–238.
[2] H. Ding, H. Pan, X. Xu, R. Tang, Toward a detailed understanding of magnesium ions on hydroxyapatite crystallization inhibition, Cryst. Growth Des. 14 (2014) 763–769.
[3] A. Nanci, Ten Cate's Oral Histology, Elsevier, 2018 9th edition ISBN: 9780-323-48524-1.
[4] J.C. Elliott, Calcium Phosphate Biominerals, Reviews in Mineralogy and Geochemistry 48 (2002) 427–453 https://doi.org/, doi:10.2138/rmg.2002.48.11.
[5] Q. Zhang, S. Gao, J. Min, D. Yu, H. Yu, Graded viscoelastic behavior of human enamel by nanoindentation, Mater Lett 179 (2016) 126–129.
[6] E. Beniash, C.A. Stifler, Ch-Y. Sun, G.S. Jung, M.J. Buehler, P.U.P.A. Gilbert, The hidden structure of human enamel, Nat. Communications 10 (2019) 4383 https://doi.org/, doi:10.1038/s41467-019-12185-7.
[7] J.D.B. Featherstone, I. Mayer, F.C.M. Driessens, R.M.H. Verbeeck, H.J.M. Heijligers, Synthetic apatites containing Na, Mg, and CO 3 and their comparison with tooth enamel mineral, Calcif Tissue Int 35 (1983) 169–171.
[8] T. Aoba, E.C. Moreno, S. Shimoda, Competitive adsorption of magnesium and calcium ions onto synthetic and biological apatites, Calcif Tissue Int 51 (1992) 143–150.
[9] C. Robinson, S.J. Brookes, R.C. Shore, J. Kirkham, The developing enamel matrix: nature and function, Eur. J. Oral. Sci. 106 (1998) 282–291.
[10] R.Z. Le Geros, T. Sakae, C. Bautista, M. Retino, J.P. Le Geros, Magnesium and carbonate in enamel and synthetic apatites, Adv. Dent. Res. 10 (1996) 225, doi:10.1177/08959374960100021801.
[11] J.L. Cuy, A.B. Mann, K.J. Livi, M.F. Teaford, T.P. Weihs, Nanoindentation mapping of the mechanical properties of human molar tooth enamel, Arch. Oral Biol. 47 (2002) 281–291.
[12] J.C. Elliott, Studies in Inorganic Chemistry, 18, Elsevier, Amsterdam, 1994.
[13] F. Ren, Y. Leng, R. Xin, X. Ge, Synthesis, characterization and ab initio simulation of magnesium-substituted hydroxyapatite, Acta Biomater 6 (2010) 2787–2796.
[14] D. Laurencin, N. Almora-Barrios, N.H. de Leeuw, C. Gervais, C. Bonhomme, F. Mauri, W. Chrzanowski, J.C. Knowles, R.J. Newport, A. Wong, Z. Gan, M.E Smith, Magnesium incorporation into hydroxyapatite, Biomaterials 32 (2011) 1826–1837.
[15] A.L. Boskey, A.S. Posner, Magnesium stabilization of amorphous Ca-phosphate: a kinetic study, Mat. Res. Bull. 9 (1974) 907–916.
[16] L.M. Gordon, M.J. Cohen, K.W. MacRenaris, J.D. Pasteris, T. Seda, D. Joester, Amorphous intergranular phases control the properties of rodent tooth enamel, Science 347 (2015) 746–750.
[17] A. La Fontaine, A. Zavgorodniy, H. Liu, R. Zheng, M. Swain, J. Cairney, Atomic-scale compositional mapping reveals Mg-rich amorphous calcium phosphate in human dental enamel, Sci. Adv. 2 (2016) e1601145.
[18] M.-N. Abdallah, H. Eimar, D.C. Bassett, M. Schnabel, O. Ciobanu, V. Nelea, M.D. McKee, M. Cerruti, F. Tamimi, Diagenesis-inspired reaction of magnesium ions with surface enamel mineral modifies properties of human teeth, Acta Biomater 37 (2016) 174–183.
[19] C.M. Zamudio-Ortega, R. Contreras-Bulnes, R.J. Scougall-Vilchis, R.A. Morales-Luckie, O.F. Olea-Mejía, L.E. Rodríguez-Vilchis, Morphological, chemical and structural characterisation of deciduous enamel: SEM, EDS, XRD, FTIR and XPS analysis, European Journal of Paediatric Dentistry 15 (2014) 275–280.
[20] U. Zilberman, S. Zilberman, D. Keinan, M. Elyiahu, Enamel development in primary molars from children with familial dysautonomia, Arch Oral Biol 55 (2010) 907–912.
[21] C. Zhou, D. Zhang, Y. Bai, S. Li, Casein phosphopeptide–amorphous calcium phosphate remineralization of primary teeth early enamel lesions, J Dent 42 (2014) 21–29.
[22] D.-G. Tocolini, M. Dalledone, J.-A. Brancher, J.-F. de Souza, C.-C. Gonzaga, Evaluation of the erosive capacity of children's beverages on primary teeth enamel: an in vitro study, J Clin Exp Dent 10 (2018) e383–e387.
[23] D.K. Whittaker, Structural variations in the surface zone of human tooth enamel observed by scanning electron microscopy, Arch Oral Biol 27 (1982) 383–392.
[24] L.W. Ripa, The histology of the early carious lesion in primary teeth with special reference to a "prismless" outer layer of primary enamel, J Dent Res 45 (1966) 5–11.
[25] T.J. White, D.Z. Li, Structural derivation and crystal chemistry of apatites, Acta Cryst B59 (2003) 1–16.
[26] B. Vincent Crist, Handbook of Monochromatic XPS spectra, Wiley, 2000.
[27] W.C. Oliver, G.M. Pharr, Measurement of hardness and elastic modulus by instrumentated indentation: advances in underatsnding and refinements to methodology, J. Mater. Res. 19 (2004) 3–20.
[28] F. Betts, A.S. Posner, An X-ray radial distribution study of amorphous calcium phosphate, Mat. Res. Bull. 9 (1974) 353–360.
[29] C. Combes, C. Rey, Amorphous calcium phosphates: synthesis, properties and uses in biomaterials, Acta Biomater 6 (2010) 3362–3378.
[30] E. Beniash, R.A. Metzler, R.S.K. Lam, P.U.P.A. Gilbert, Transient amorphous calcium phosphate in forming enamel, J. Struct. Biol. 166 (2009) 133–143.
[31] L.M. Gordon, D. Joester, Mapping residual organics and carbonate at grain boundaries and amorphous interphase in mouse incisor enamel, Front. Physiol. 6 (2015) 57, doi:10.3389/fphys.2015.00057.
[32] W.L. Suchanek, K. Byrappa, P. Shuk, R.E. Riman, V.F. Janas, K.S. Ten-Huisen, Preparation of magnesium-substituted hydroxyapatite powders by the mechanochemical-hydrothermal method, Biomaterials 25 (2004) 4647–4657.
[33] S. Cazalbou, D. Eichert, X. Ranz, C. Drouet, C. Combes, M.F. Harmand, C. Rey, Ion exchanges in apatites for biomedical applications, J. Mat. Sci.: Materials in medicine 16 (2005) 405–409.
[34] C. Drouet, M.-T. Carayon, C. Combes, C. Rey, Surface enrichment of biomimetic apatites with biologically-active ions Mg^{2+} and Sr^{2+}: a preamble to the activation of bone repair materials, Mat. Sci. Eng. C 28 (2008) 1544–1550.
[35] L. Bertinetti, C. Drouet, C. Combes, C. Rey, A. Tampieri, S. Coluccia, G. Martra, Surface characteristics of nanocrystalline apatites: effect of Mg surface enrichment on morphology, surface hydration species, and cationic environments, Langmuir 25 (2009) 5647–5654.
[36] D. Lee, P.M. Kumta, Chemical synthesis and characterization of magnesium substituted amorphous calcium phosphate (MG-ACP), Mat. Sci. .Eng. C 30 (2010) 1313–1317.
[37] C. Drouet, M. Aufray, S. Rollin-Martinet, N. Vandecandelaere, D. Grossin, F. Rossignol, E. Champion, A. Navrotsky, C. Rey, Nanocrystalline apatites: the fundamental raw of water, Am. Miner. 103 (2018) 550–564.
[38] J.C. Elliott, Structure, crystal chemistry and density of enamel apatites, in: D.J. Chadwick, G. Cardew (Eds.), Dental enamel, Wiley, 2007 ISBN: 978-0-470-51530-3.
[39] P.B. Barna, M. Adamik, Fundamental structure forming phenomena of polycrystalline films and the structure zone models, Thin Solid Films 317 (1998) 27–33.
[40] D.R. Clarke, On the equilibrium thickness of intergranular glass phases in ceramic materials, J. Am. Ceram. Soc. 70 (1987) 15–22.
[41] J. Koldehoff, M.W. Swain, G.A. Schneider, The geometrical structure of interfaces in dental enamel: a FIB-STEM investigation, Acta Biomater 104 (2020) 17–27.
[42] A. Makishima, J.D. Mackenzie, Direct calculation of Young's modulus of glass, J. Non-Cryst. Solids 12 (1973) 35–45.
[43] Y.T. Cheng, C.M. Cheng, Scaling, dimensional analysis, and indentation measurements, Mater. Sci. Eng. R 44 (2004) 91–149.
[44] J.P. Sun, Y. Song, G.W. Wen, Y. Wang, R. Yang, Softening of hydroxyapatite by vacancies: a first principles investigation, Mater. Sci. Eng. C 33 (2013) 1109–1115.